Controlling water exchange rates in potential Mn^{2+}-based MRI agents derived from NO2A^{2-} [i]

Rosa Pujales-Paradela[a], Fabio Carniato[b], David Esteban-Gómez[a], Mauro Botta[b*] and Carlos Platas-Iglesias[a†]

[a] Universidade da Coruña, Centro de Investigacións Científicas Avanzadas (CICA) and Departamento de Química, Facultade de Ciencias, A Coruña, Galicia, Spain

[b] Dipartimento di Scienze e Innovazione Tecnologica, Università del Piemonte Orientale "A. Avogadro", Viale T. Michel 11, 15121 Alessandria, Italy

Abstract

We report a series of pentadentate ligands based on a 1,4,7-triazacyclononane-1,4-diacetic acid (H$_2$NO2A) containing different substituents attached to the third nitrogen atom of the macrocyclic unit. Detailed ^{1}H Nuclear Magnetic Relaxation Dispersion (NMRD) characterisation of the corresponding Mn^{2+} complexes suggests the formation of six-coordinate species in solution containing an inner-sphere water molecule. This was confirmed by recording the transverse ^{17}O relaxation time and chemical shift measurements. The water exchange rate of the coordinated water molecule was found to be strongly influenced by the nature of the substituent R at position 7 of the triazacyclononane unit (R = Me, k^{298}_{ex} = 62.6 × 10^7 s^{-1}; R = Bz, k^{298}_{ex} = 4.4 × 10^7 s^{-1}; R = 1-phenylethyl, k^{298}_{ex} = 2.6 × 10^7 s^{-1}). The decreasing exchange rates are explained by the increasing bulkiness of the substituent, which hinders the approach of the entering water molecule in an associatively activated water exchange mechanism. This is supported by DFT calculations (M062X/TZVP), which confirm the associative nature of the water exchange reaction. A potentially decadentate ligand containing two NO2A units linked by a xylenyl spacer in the *meta* position was also synthesised. The corresponding binuclear Mn^{2+} complex contains two metal ions with different hydration numbers, as evidenced by ^{1}H NMRD and ^{17}O NMR measurements. DFT calculations show that this is related to the presence of a bridging bidentate μ–η^1-carboxylate group connecting the two metal centers. The results reported in this work provide a straightforward strategy to control the exchange rate of the coordinated water molecule in this family of MRI contrast agent candidates.

Introduction

Magnetic Resonance Imaging (MRI) has emerged over the last few decades as one of the most successful and widely used diagnostic imaging modalities, and nevertheless is under continuous development and

---

* mauro.botta@uniupo.it
† carlos.platas.iglesias@udc.es

improvement. Contrast agents (CA) are broadly used during the MRI scans in order to improve the contrast in the recorded images of organs and tissues, increasing the sensitivity and decreasing the acquisition times.[1] These agents are usually paramagnetic metal complexes with good water solubility that increase the relaxation rates of water proton nuclei in their vicinity.[1,2] One of the most common and widespread CAs used in clinical practice is DOTAREM®, a Gd^{3+} macrocyclic complex that presents high stability and relaxivity.[1] In the last few years, renewed interest has emerged to find alternatives to the already used Gd^{3+} chelates, because of the rising concerns about some health risks associated with their use.[3] Although none of the studies reported so far demonstrated a clinically relevant toxic effect directly attributed to gadolinium deposition in brain and other tissues,[4] gadolinium contrast agents are related to the onset of nephrogenic systemic fibrosis (NSF) in patients with abnormal and even normal renal function, or those who have experienced liver transplantation.[3] Several suspensions of marketing authorizations and restrictions in the use of linear gadolinium-based contrast agents have been executed recently by some international regulatory health authorities,[5] and these restrictions are likely to be expanded in the near future.

In this renewed interest on alternatives to gadolinium contrast agents, high-spin manganese(ii) complexes play a strong leading role,[6–9] due to a number of optimal features: a high effective magnetic moment associated with the presence of five unpaired d electrons, a long electronic relaxation time and fast water exchange kinetics.[6] In recent papers, we have reported several manganese systems that present relatively high relaxivities, comparable to those of small monohydrated Gd^{3+} complexes.[10] These chelates should guarantee high thermodynamic and kinetic stability to avoid the release of the Mn^{2+} ion *in vivo*,[11] and they should present one free coordination site of the metal ion for at least one water molecule. Besides, the ligands should provide good redox stability to avoid the oxidation of Mn^{2+} to Mn^{3+}, which commonly furnishes lower relaxivities.[12] It is worth noting that it has been proven that contrast agents based on macrocyclic metal complexes are generally kinetically more inert than linear analogues.[13]

Among the different parameters that affect the efficiency (relaxivity) of Mn^{2+}-based contrast agents, the exchange rate of the coordinated water molecule(s) plays an important key role. Some time ago, É. Tóth and co. reported detailed characterisation of the NO2A derivative [Mn2(ENOTA)] (Scheme 1), which was found to exhibit a rather slow water exchange rate of the coordinated water molecule (k^{298}_{ex} = 5.5 × 10^7 s^{-1}),[14] comparable to that of the aquated $[Mn(H_2O)_6]^{2+}$ ion (k^{298}_{ex} = 2.8 × 10^7 s^{-1}).[15] In a subsequent study, we investigated the [Mn(MeNO2A)] complex, which was found to present a water exchange rate one order of magnitude higher (k^{298}_{ex} = 62.6 × 10^7 s^{-1}).[16] Other [Mn(NO2A)] derivatives containing different pendant arms attached to the third N atom of the macrocyclic unit presented k^{298}_{ex} values in the range 1.3–2.7 × 10^7 s^{-1}.[17]
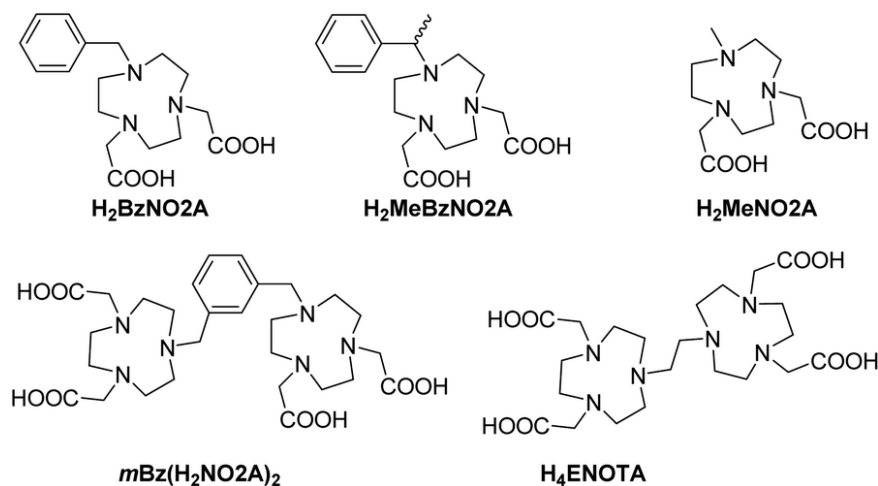

Scheme 1. Chemical structures of the ligands studied in this work.

The motivation of this study was to analyse the effect that steric hindrance causes in the water exchange rate of [Mn(NO2A)] derivatives. We hypothesised that the presence of bulky groups in the vicinity of the water binding site may hinder the approach of a water molecule from the bulk, following an associatively activated mechanism. To this aim, we prepared H$_2$BzNO2A and H$_2$MeBzNO2A ligands (Scheme 1) and performed full relaxometric characterisation of the corresponding Mn^{2+} complexes using Nuclear Magnetic Relaxation Dispersion (NMRD)[18] and ^{17}O NMR studies. The different bulkiness of the groups attached to the secondary amine of NO2A and a comparison with [Mn(MeNO2A)] allows the rationalisation of the water exchange dynamics in this family of complexes. Furthermore, we also report here the binuclear complex [*m*Bz(MnNO2A)$_2$], in an attempt to increase the observed relaxivity by slowing down the molecular tumbling of the complex in solution.

Results and discussion

<u>Synthesis</u>

The triazacyclononane-based ligands H$_2$BzNO2A, H$_2$MeBzNO2A and *m*Bz(H$_2$NO2A)$_2$ were prepared by alkylation of the bis-protected triazacyclononane derivative di-*tert*-butyl 2,2′-(1,4,7-triazacyclononane-1,4-diyl)diacetate (NO2A*t*Bu) with alkyl bromide derivatives **1a**, **1b** or **1c** (Scheme 2). The protected ligands were isolated in quantitative yields, and then treated with TFA to remove the *tert*-butyl protecting groups. The final ligands were isolated in nearly quantitative amounts.
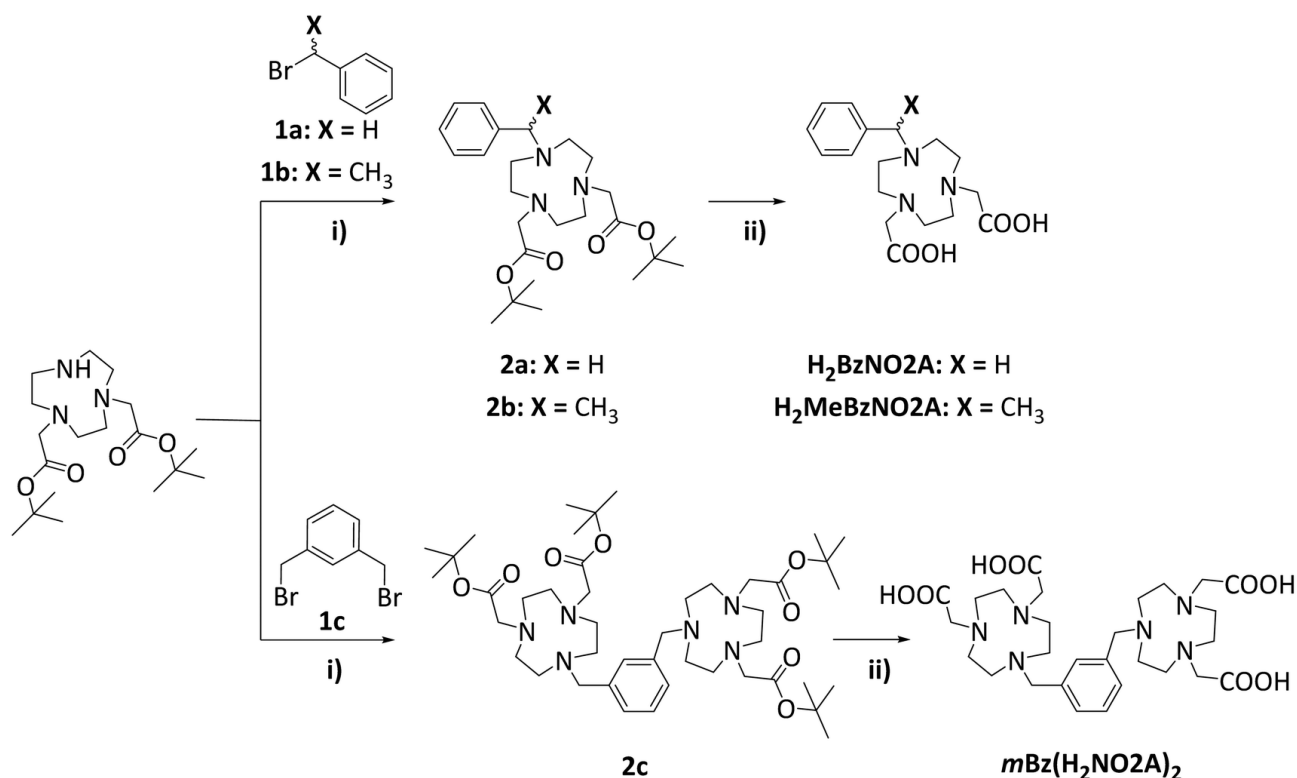
Scheme 2. Synthesis of the ligands discussed in this work. Conditions: (i) K$_2$CO$_3$ in CH$_3$CN, 48 h, 100%; (ii) TFA : CH$_2$Cl$_2$, RT, 48 h, 88–100%.

The preparation of the Mn^{2+} complexes was carried out by a solvothermal approach using *n*-butanol as the solvent and DIPEA as the base. The complexes were purified by reverse-phase medium pressure liquid

chromatography (MPLC). The high-resolution mass spectra (ESI$^+$, Fig. S13–S15, ESI[i]) confirm the formation of the complexes.

<u>pH dependence of ^{1}H relaxivity (r_{1p})</u>

The efficiency of a paramagnetic complex as a contrast agent *in vitro* is determined from its relaxivity, r_{1p}, defined as the relaxation enhancement of water protons induced by the paramagnetic agent at a 1 mM concentration (based on the paramagnetic metal ion).

The relaxivity determined for [Mn(BzNO2A)] at pH 6.47 (25 °C, 20 MHz) is 3.43 mM^{-1} s^{-1}, a value that is close to that reported for monohydrated complexes of similar sizes, such as [Mn(EDTA)]$^{2-}$ (3.3 mM^{-1} s^{-1} at pH 7.4, 25 °C and 20 MHz).[19] The r_{1p} value measured for [Mn(MeBzNO2A)] under the same conditions (3.54 mM^{-1} s^{-1}) is very similar, indicating a low impact of the added methyl group on the observed relaxivity. These relaxivity values suggest the presence of a water molecule coordinated to the metal ion in both [Mn(BzNO2A)] and [Mn(MeBzNO2A)], indicating that the presence of the methyl group does not affect the hydration state of the complex. Meanwhile, the relaxivity measured for the dinuclear chelate [*m*Bz(MnNO2A)$_2$] (2.58 mM^{-1} s^{-1}) is clearly lower than those of the related mononuclear complexes. However, this relaxivity is still higher than the one observed for non-hydrated Mn^{2+} complexes such as [Mn(DO3A)]$^-$,[19] but close to the r_{1p} values reported for complexes with $0 < q < 1$ (q is the number of coordinated water molecules).[20] Thus, the relaxivity measured for [*m*Bz(MnNO2A)$_2$] suggests that the coordination environment of at least one of the Mn^{2+} ions differs with respect to those of the mononuclear analogues.

The relaxivities of the three complexes (25 °C, 20 MHz) were measured over a broad pH range, from 3 to 12, to assess their stability around physiological pH (Fig. 1). The observed relaxivities are constant in the pH range ∼6.0–9.0. Below that range relaxivity increases due to the stepwise dissociation of the complex and formation of [Mn(H$_2$O)$_6$]$^{2+}$, which presents a relaxivity of 8.6 mM^{-1}s^{-1} under these conditions.[15b] Above pH ∼9, r_{1p} experiences a significant increase, which might be related to an acceleration of the water exchange process by a base-catalysed mechanism. A relaxivity increase at high pH values was observed previously for lanthanide complexes presenting slow water exchange thanks to the prototropic base-catalysed mechanism.[21,22] Since water exchange in these [Mn(NO2A)] derivatives is rather fast and does not limit relaxivity at 298 K (see below), the relaxivity increase at basic pH must be related to a different effect. It has been shown that [Mn(NO2A)] complexes form hydroxo species at basic pH.[17] Thus, the formation of hydroxo species is most likely responsible for the observed behaviour, by affecting the number of proton nuclei in the vicinity of the metal ion, the Mn⋯H distance or the rotational dynamics of the complex.
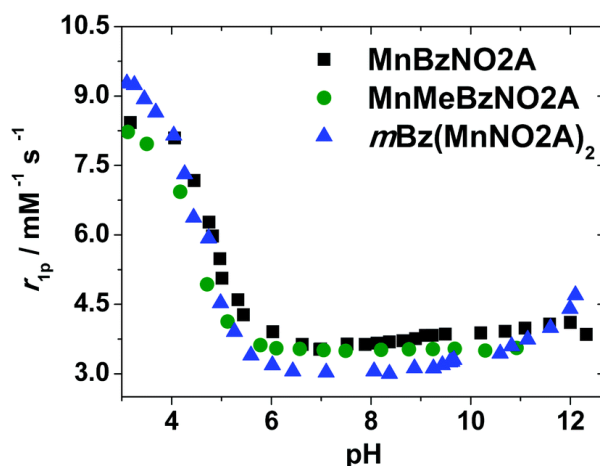

Fig. 1. Plot of the ^{1}H relaxivities at 20 MHz and 298 K as a function of pH.
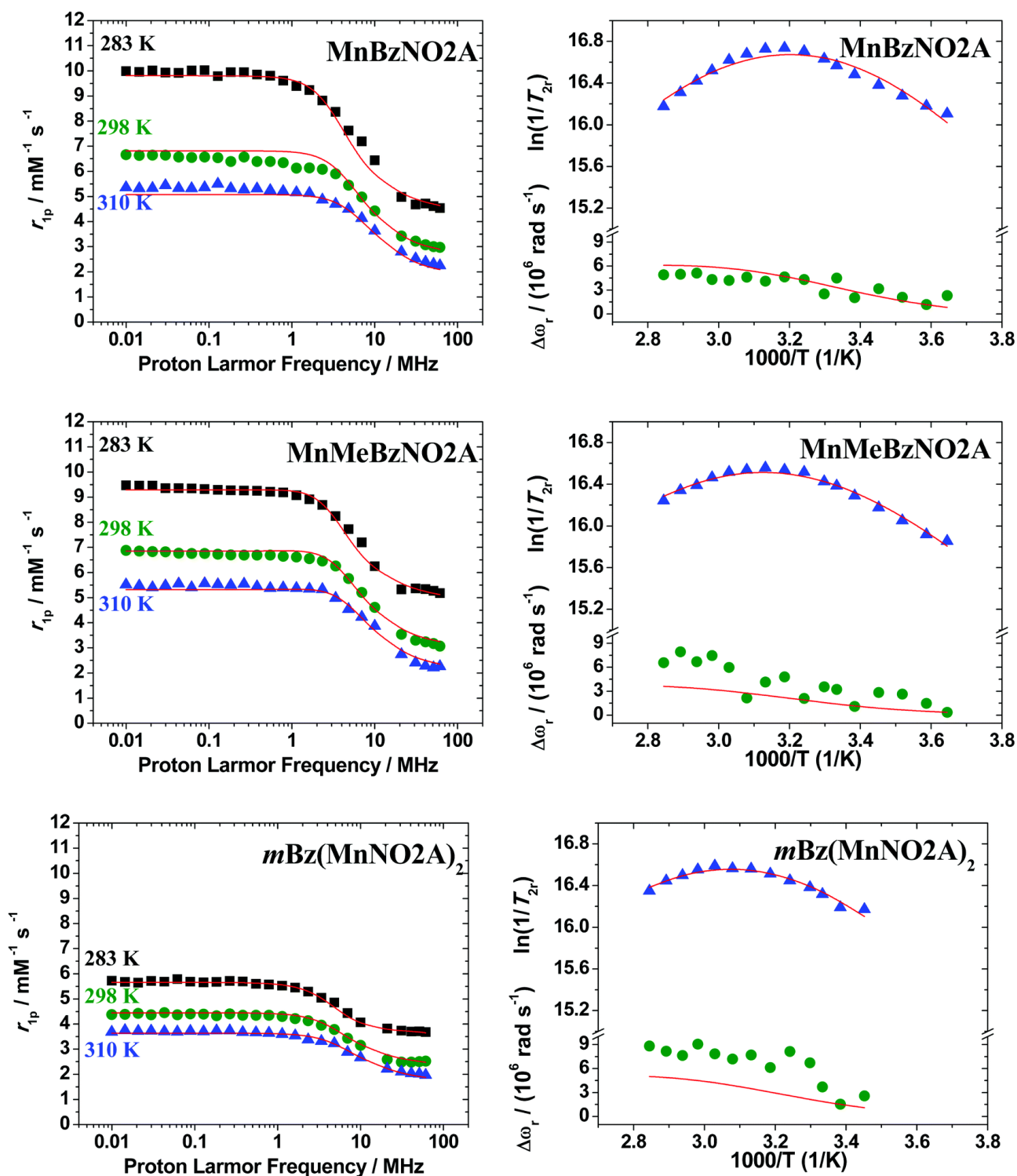
Fig. 2. Left panel: ^{1}H NMRD profiles recorded at different temperatures for [Mn(BzNO2A)], [Mn(MeBzNO2A)] and [*m*Bz(MnNO2A)$_2$]. Right panel: Reduced transverse ^{17}O NMR relaxation rates and chemical shifts *versus* reciprocal temperature. The red lines represent the fitting of the data as explained in the text.

<u>^{1}H NMRD measurements</u>

Proton Nuclear Magnetic Relaxation Dispersion (^{1}H NMRD) profiles were recorded at 10, 25 and 37 °C in the proton Larmor frequency range from 0.01 to 70 MHz. The analysis of the ^{1}H NMRD profiles provides additional information on the different mechanisms and physicochemical parameters that affect the observed relaxivity (Fig. 2). The NMRD profiles recorded for [Mn(BzNO2A)] and [Mn(MeBzNO2A)] are nearly

identical in the whole range of [1]H Larmor frequencies, which suggests that the two complexes present very similar structures and dynamics. The relaxivities of the dinuclear complex [*m*Bz(MnNO2A)$_2$] are clearly lower, again suggesting a lower hydration number. The NMRD profiles recorded for the three complexes present a single dispersion in the range ~2–20 MHz and two plateaus at low (<2 MHz) and high (>20 MHz) fields. The relaxivity at a high field decreases with an increase in temperature in all cases, a situation typical of small Mn^{2+} chelates presenting fast rotation (short rotational correlation times, τ_R).[18] It is also worth mentioning that the NMRD profiles do not show a second dispersion at a low field (~0.3–0.02 MHz), which is characteristic of complexes that present a sizeable scalar contribution to relaxivity. This second dispersion was so far only observed for the aquated ion [Mn(H$_2$O)$_6$]$^{2+}$ and [Mn$_2$(ENOTA)].[14,15]

Recently, Peters and Geraldes have proposed a method to determine the hydration number of Mn^{2+} complexes from ^{1}H NMRD measurements.[23] These authors proposed a correlation of the hydration number q with the relaxivity observed at 0.01 MHz (and 25 °C) and the molecular weight (FW) of the complex:

$$q = \frac{r_{1p}}{9.16\left\{1-e^{(-2.97\times FW\times 10^{-3})}\right\}} \tag{1}$$

The relaxivities at 0.01 MHz and 25 °C were determined to be 4.97, 6.63, 6.88 and 4.38 mM^{-1} s^{-1} for [Mn(MeNO2A)], [Mn(BzNO2A)], [Mn(MeBzNO2A)] and [*m*Bz(MnNO2A)$_2$], which correspond to q values of 0.9, 0.9, 1.1 and 0.5. The estimated uncertainty of the method was determined to be ±0.4 units. These results point to the formation of monohydrated species for all mononuclear complexes of this series, while the dinuclear complex [*m*Bz(MnNO2A)$_2$] likely presents a lower effective hydration number.

^{17}O NMR measurements

Transverse ^{17}O NMR relaxation rate measurements were recorded at 11.75 T to obtain information regarding the hydration number and water exchange rate of the coordinated water molecule ($k_{ex} = 1/\tau_m$). The paramagnetic [17]O transverse relaxation rates $1/T_{2p}$ can be approximated using:

$$\frac{1}{T_{2p}} = \frac{1}{T_{2,obs}} - \frac{1}{T_{2,ref}} = \frac{q[Mn^{2+}]}{[H_2O]}\frac{1}{\tau_m}\frac{T_{2m}^{-2}+\tau_m^{-1}T_{2m}^{-1}+\Delta\omega_m^2}{\left(\tau_m^{-1}+T_{2m}^{-1}\right)^2+\Delta\omega_m^2} \tag{2}$$

where $1/T_{2,obs}$ and $1/T_{2,ref}$ are the observed relaxation rates for the solution of the paramagnetic complex and of the diamagnetic reference, respectively, while $1/T_{2m}$ is the relaxation rate of the bound water molecule. By neglecting the chemical shift difference between bound and bulk water ($\Delta\omega_m$), the $1/T_{2p}$ values can be approximated as:

$$\frac{1}{T_{2p}} = \frac{q[Mn^{2+}]}{[H_2O]}\frac{1}{\tau_m+T_{2m}} \tag{3}$$

The ^{17}O transverse relaxation rate of the coordinated water molecule is dominated by the scalar mechanism according to:

$$\frac{1}{T_{2m}} \cong \frac{1}{T_{2,sc}} = \frac{S(S+1)}{3}\left(\frac{A}{\hbar}\right)^2 \tau_{S1} \tag{4}$$

Here, $A/\hbar$ is the scalar hyperfine coupling constant and S is the electron spin ($S = 5/2$ for a high-spin Mn^{2+} complex). $1/\tau_{s1}$ is the sum of the exchange rate constant and the electron spin relaxation rate:

$$\frac{1}{\tau_{S1}} = \frac{1}{\tau_m} + \frac{1}{T_{1e}} \tag{5}$$

Caravan *et al.*[24] noticed that at high magnetic fields $T_{1e} \gg \tau_m$, so that τ_m is the correlation time that dominates in eqn (4). As a result, at the maximum of the temperature dependence of $1/T_{2p}$, where $T_{2m} = \tau_m$, one can obtain eqn (6) by combining eqn (3) and (4):

$$q = r_{2p,max}[H_2O]\left(\frac{2}{\sqrt{\frac{S(S+1)}{3}\frac{A_O}{\hbar}}}\right) \tag{6}$$

In eqn (6) r_{2p} stands for the transverse ^{17}O relaxivity, defined as:

$$\frac{1}{T_{2p}} = r_{2p}[Mn^{2+}] \tag{7}$$

The temperature dependence of r_{2p} measured for the three complexes shows that [Mn(BzNO2A)] and [Mn(MeBzNO2A)] present very similar transverse relaxivities at the maximum of the temperature dependence ($r_{2p} \sim 300$ mM^{-1} s^{-1}, Fig. 3), while the relaxivity measured for [mBz(MnNO2A)$_2$] is about one half of those observed for the mononuclear complexes ($r_{2p} \sim 150$ mM^{-1} s^{-1}). Thus, these results indicate that the binuclear [mBz(MnNO2A)$_2$] complex presents a lower hydration number than the mononuclear analogues. By assuming a $A/\hbar$ value of -33×10^6 rad s^{-1}, Caravan proposed that each coordinated water molecule should provide a contribution of 510 mM^{-1} s^{-1} to r_{2p}. This results in hydration numbers of $q = 0.6$ for the mononuclear complexes and $q = 0.3$ for [mBz(MnNO2A)$_2$]. Since the proton relaxivities point to the presence of a coordinated water molecule in [Mn(BzNO2A)] and [Mn(MeBzNO2A)], we conclude that our ^{17}O r_{2p} measurements underestimate the hydration number of these complexes. We attribute this to the fact that the approximations described above are not completely fulfilled. Indeed, neglecting the chemical shift difference between bound and bulk water ($\Delta\omega_m$) in eqn (2) affects the transverse relaxation rates

significantly (Fig S16, ESI$^+$†). Furthermore, the assumption that $T_{1e} \gg \tau_m$ may also not be completely valid. For instance, the water exchange rate obtained for [Mn(BzNO2A)] at the maximum observed in Fig. 3 (~9 × 10^7 s^{-1}) is in the same order of magnitude as the value of T_{1e} obtained from simulations of the transient zero field splitting in [Mn(MeNO2A)] (~1 × 10^7 s^{-1}).[25] Thus, taken together, the ^{17}O and ^{1}H data are compatible with $q = 1$ mononuclear complexes and a $q = 0.5$ dinuclear [mBz(MnNO2A)$_2$] complex. Our DFT calculations presented below provide support to this hypothesis.
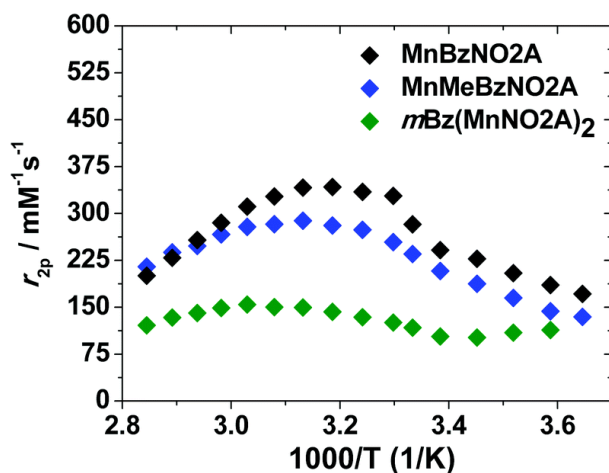

Fig. 3. Plot of the transverse ^{17}O relaxivity as a function of temperature recorded at 11.75 T.

With the hydration numbers in hand, we obtained the reduced transverse relaxation rates (1/T_{2r}), which are normalised for the molar fraction of bound water P_m:

$$\frac{1}{T_{2r}} = \frac{1}{P_m} \left[\frac{1}{T_{2,obs}} - \frac{1}{T_{2,ref}} \approx \frac{1}{\tau_m + T_{2m}} \right] \tag{8}$$

The temperature dependence of T_{2m} and τ_m are generally opposite, so that the residence time of the coordinated water molecule is shortened on increasing the temperature (*i.e.* k_{ex} increases), while the T_{2m} becomes longer. Thus, the plots of 1/T_{2r} *versus* reciprocal temperature present different slopes depending on the term that dominates the denominator of eqn (2). A positive slope is then expected in the plots of 1/T_{2r} *versus* 1/T for systems in the fast exchange regime, while the opposite behaviour should be observed for complexes within the slow exchange regime. In the case of the complexes investigated here, the 1/T_{2r} data present a maximum that points to a changeover from the low water exchange regime at low temperatures to a fast water exchange at high temperatures (Fig. 2). This temperature dependence of 1/T_{2r} is in clear contrast to that observed for [Mn(MeNO2A)], which was characterised by a very fast water exchange.[16] We also notice that the maximum of 1/T_{2r} is shifted towards higher temperatures for [mBz(MnNO2A)$_2$] and [Mn(MeBzNO2A)] with respect to [Mn(BzNO2A)], which indicates a slightly faster water exchange in the latter.

Fitting of the ^{17}O NMR and ^{1}H NMRD data

A quantitative analysis of the ^{17}O and ^{1}H NMRD data was carried out using the Solomon–Bloembergen–Morgan theory to describe the inner-sphere contribution[26] and Freed's model[27] to account for the outer-sphere

contribution to relaxivity. The complete set of equations used, together with those describing the ^{17}O NMR data, are given in the ESI.† These equations depend upon a large number of parameters; hence to achieve a reliable analysis some of them had to be fixed to standard values during the fitting procedure: the distances between the proton nuclei of inner-sphere water molecules and the metal ion (r_{MnH}) were fixed to the average values obtained from DFT calculations (Table 1), while the distance of closest approach of outer-sphere water molecules a_{MnH} was set at 3.6 Å. Finally, the diffusion coefficient D^{298}_{MnH} and the activation energy E_{DMnH} were fixed to established values.[19] Table 1 shows the parameters obtained from the fitting, which are compared with those reported previously for [Mn(MeNO2A)] and [Mn$_2$(ENOTA)].[14,16]

Table 1. Parameters obtained from the simultaneous analysis of ^{17}O NMR and ^{1}H NMRD data^a.

	[Mn(BzNO2A)]	[Mn(MeBzNO2A)]	[mBz(MnNO2A)$_2$]	[Mn(MeNO2A)]^b	[Mn$_2$(ENOTA)]^c
r_{1p} at 10/25/37 °C/mM^{-1} s^{-1}	5.0/3.4/2.8	5.3/3.5/2.7	3.8/2.6/2.2	3.3/2.8	
$k^{298}_{ex}/10^7$ s^{-1}	4.4 ± 0.1	2.6 ± 0.1	2.4 ± 0.1	62.6 ± 2.3	5.5
$\Delta H^{\ddagger}$/kJ mol^{-1}	32.17 ± 1.5	25.4 ± 0.9	31.1 ± 1.6	11 ± 1.0	20.5
$\Delta S^{\ddagger}$/J mol^{-1} K^{-1}	−27 ± 8	−10 ± 6	−23 ± 7		−28
τ^{298}_R/ps	52.8 ± 0.1	67.2 ± 0.6	78.7 ± 0.7	36 ± 3	85
E_r/kJ mol^{-1}	26.7 ± 0.8	24.6 ± 0.5	20.8 ± 0.6	22.8 ± 0.7	18
τ^{298}_V/ps	51 ± 4	52 ± 4	25 ± 2	21.4 ± 3.8	7.7
E_v/kJ mol^{-1}	1.0^a	1.0^a	1.0^a	1.0^a	24.8
$D^{298}_{MnH}/10^{-10}$ m^2 s^{-1}	20.0^a	20.0^a	20.0^a	26.9 ± 4.0	23.0^a
E_{DMnH}/kJ mol^{-1}	20	20	20	17.3 ± 2.4	18
$\Delta^2/10^{19}$ s^{-2}	1.69 ± 0.08	2.26 ± 0.11	6.9 ± 0.4	7.2 ± 1.5	0.47
$A_O/\hbar^d/10^6$ rad s^{-1}	−49.6 ± 2.3	−32.6 ± 0.9	−44.1 ± 2.7	−46.0 ± 0.2	−32.7
$A_O/\hbar^e/10^6$ rad s^{-1}	−51.3	−52.0		−52.3	
r_{MnH}/Å	2.85^a	2.865^a	2.85^a	2.77^a	2.75
a_{MnH}/Å	3.6^a	3.6^a	3.6^a	3.6^a	3.2
q^{298}	1^a	1^a	0.5^a	1^a	1

^{a} Parameters fixed during the fitting procedure. ^{b} Data from ref. 16. ^{c} Data from ref. 14. ^{d} Experimental values obtained from ^{17}O NMR measurements. ^{e} Obtained with DFT calculations.

The ^{17}O hyperfine coupling constants ($A_O/\hbar$) are in the upper part of the range typically observed for small Mn^{2+} complexes (25 × 10^6 to 47 × 10^6 rad s^{-1}).[28] Furthermore, they are in very good agreement with the values estimated by DFT calculations (see below), which confirms that the hydration numbers used in the analysis are correct.

The rotational correlation times (τ^{298}_R) obtained for [Mn(BzNO2A)] and [Mn(MeBzNO2A)] are very similar, but somewhat longer than the value reported previously for [Mn(MeNO2A)], as would be expected on the basis of their molecular weights. The τ^{298}_R value obtained for [mBz(MnNO2A)$_2$] is about 50% higher than that of [Mn(MeNO2A)], matching rather well that of [Mn$_2$(ENOTA)] (Table 1).

The parameters related to the relaxation of the electron spin of the Mn^{2+} ion (the mean square zero-field-splitting energy (Δ^2) and its associated correlation time (τ_V)) are similar to the values reported for other Mn^{2+} complexes. The mononuclear complexes [Mn(BzNO2A)] and [Mn(MeBzNO2A)] present very similar parameters, which suggests very similar coordination environments of the metal ion in the two complexes. The value of Δ^2 obtained for [mBz(MnNO2A)$_2$)] is somewhat higher, but very similar to that of [Mn(MeNO2A)].

The water exchange rates determined for this family of complexes match the qualitative analysis presented in the previous section. The water exchange rate determined for [Mn(BzNO2A)] ($k^{298}_{ex} = 4.4 \times 10^7 \, s^{-1}$) is one order of magnitude lower than that obtained for [Mn(MeNO2A)] ($k^{298}_{ex} = 63 \times 10^7 \, s^{-1}$). These very different k^{298}_{ex} values highlight the impact that an increasing steric hindrance has on the water exchange rate. Increasing further the steric hindrance by introducing a methyl group at the benzylic carbon reduces further the water exchange rate ($k^{298}_{ex} = 2.6 \times 10^7 \, s^{-1}$ for [Mn(MeBzNO2A)]). Finally, the binuclear complex [*m*Bz(MnNO2A)$_2$] displays a water exchange rate similar to that of [Mn(MeBzNO2A)]. The activation entropies obtained from the fit of the ^{17}O NMR data are negative and very close to that reported for [Mn$_2$(ENOTA)], in line with an associatively activated water exchange reaction.[14]

Theoretical calculations

DFT calculations (M062X/TZVP) were carried out to gain information on the structures of the complexes described in this work and their water exchange kinetics. The [Mn(MeNO2A)] complex was studied with DFT calculations in a previous report including a coordinated water molecule and a variable number of explicit second-sphere water molecules.[16] These studies showed that the inclusion of two second-sphere water molecules was critical for an adequate description of the Mn–O$_{water}$ distances and scalar hyperfine coupling constants $A_O/\hbar$. We therefore included two explicit second-sphere water molecules in our models. In the case of the complex of *m*Bz(MnNO2A)$_2$ the experimental ^{1}H NMRD and ^{17}O NMR data suggest the presence of a water molecule coordinated to one of the Mn^{2+} ions, while the second one does not contain a coordinated water molecule. We hypothesised that a carboxylate group of one of the NO2A units of the ligand could coordinate simultaneously to the two Mn^{2+} ions, as bridging carboxylate groups were observed previously in the solid state structures of Mn^{2+} complexes with polyaminopolycarboxylate ligands.[29] The optimised geometry of the [*m*Bz(MnNO2A)(MnNO2A)(H$_2$O)]·2H$_2$O system (Fig. 4) supports the different hydration numbers of the two Mn^{2+} ions, as a result of the presence of a bridging bidentate μ–η^1-carboxylate group.
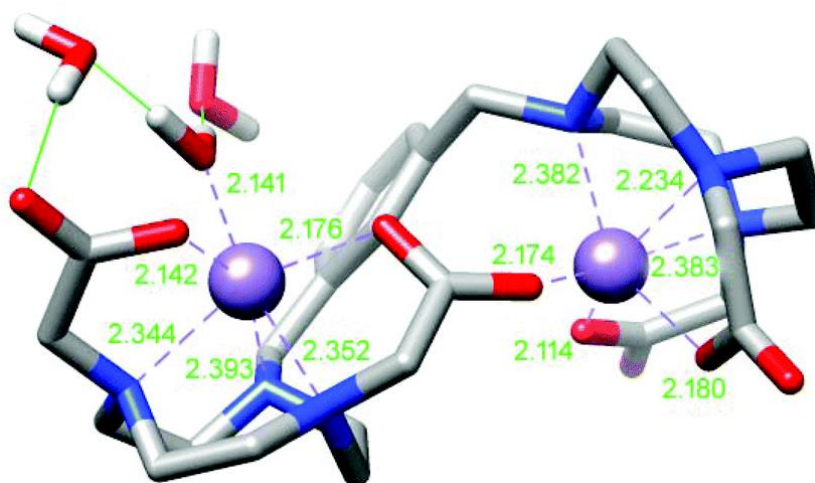

Fig. 4. Structure of the [mBz(MnNO2A)(MnNO2A)(H$_2$O)]·2H$_2$O system obtained with DFT calculations (M062X/TZVP). Bond distances are provided in Å.

The Mn–O$_{water}$ distances calculated for [Mn(MeNO2A)(H$_2$O)]·2H$_2$O, [Mn(BzNO2A)(H$_2$O)]·2H$_2$O and [Mn(MeBzNO2A)(H$_2$O)]·2H$_2$O are virtually identical (2.183–2.185 Å), while for the [*m*Bz(MnNO2A)(MnNO2A)(H$_2$O)]·2H$_2$O system this distance is slightly shorter (2.141 Å). The scalar hyperfine coupling constants $A_O/\hbar$ obtained with DFT for [Mn(MeNO2A)(H$_2$O)]·2H$_2$O,

[Mn(BzNO2A)(H$_2$O)]·2H$_2$O and [Mn(MeBzNO2A)(H$_2$O)]·2H$_2$O are also very similar ($\sim$$-50 \times 10^6$ rad s^{-1}), and show satisfactory agreement with the experimental values, though the deviation is more important in [Mn(MeBzNO2A)(H$_2$O)]·2H$_2$O. These results confirm that the hydration numbers assumed for the analysis of the ^{1}H NMRD and ^{17}O NMR data are correct, and that the bulkiness of the substituents attached to position 7 of the triazacyclononane unit does not significantly influence the strength of the Mn–O$_{water}$ bonds.

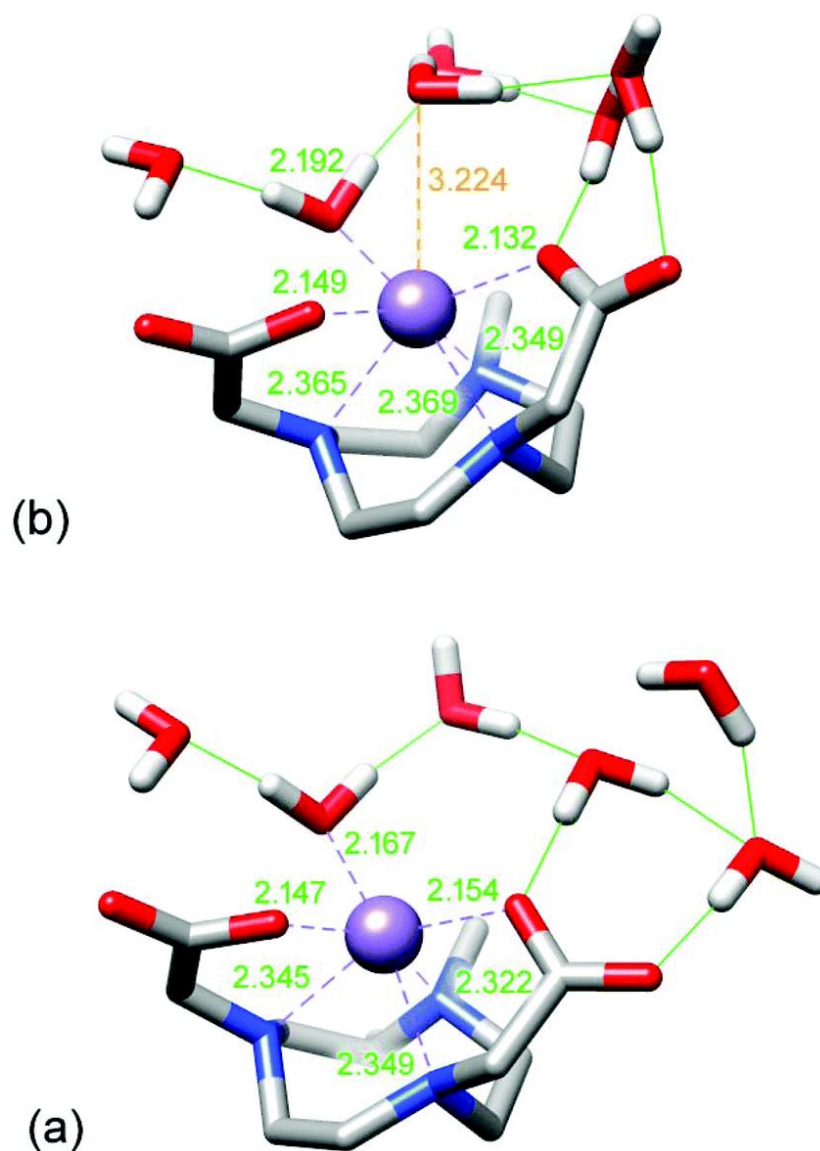**Fig. 5.** Structures of the energy minimum (a) and transition state (b) characterising the associative water exchange mechanism in [Mn(MeNO2A)(H$_2$O)]·5H$_2$O (M062X/TZVP). Bond distances are provided in Å.

Additional DFT calculations were performed to gain insight into the mechanism responsible for the water exchange reaction in this family of complexes.[30] For this purpose, we used a model of the [Mn(MeNO2A)] complex including six explicit water molecules. We then optimised the geometries of the [Mn(MeNO2A)(H$_2$O)]·5H$_2$O and [Mn(MeNO2A)(H$_2$O)$_2$]·4H$_2$O systems (Fig. 5), which turned out to correspond to the local energy minima of the potential energy surface. Our calculations predict that the monohydrated complex is more stable than the $q = 2$ complex, with a Gibbs free energy difference of 7.2 kJ mol^{-1}. Thus, our calculations with the M062X functional predict the correct hydration number for the

[Mn(MeNO2A)] complex, in line with recent findings.[31] Next we located the transition state connecting the two energy minima, which provided an activation free energy of $\Delta G^{\#298} = 7.6$ kJ mol^{-1}. The distance between the metal ion and the entering water molecule decreases from 6.01 to 3.22 Å to reach the transition state, while the Mn–O distance involving the coordinated water molecule experiences only a slight increase from 2.17 to 2.19 Å, in line with an associatively activated mechanism. The calculated activation entropy is negative ($\Delta S^{\#} = -47.3$ J mol^{-1} K^{-1}), as would be expected for an associative mechanism,[32] representing the main contribution to the free energy barrier at 298 K.

Conclusions

In this work, we have presented a family of Mn^{2+} complexes with ligands containing a NO2A^{2-} chelating unit functionalised with different substituents at the third nitrogen atom of the triazacyclononane moiety. A detailed relaxometric study showed that the water exchange process becomes slower upon increasing the steric hindrance around the water binding site. This can be accounted for by the associative mechanism followed by the water exchange process. The increased bulkiness of the substituent hinders the approach of the entering water molecule, causing destabilisation of the seven-coordinated transition state. DFT calculations provided support for the associative water exchange mechanism.

The results reported here give insight at the molecular level into important parameters that control the efficiency of Mn^{2+} complexes as MRI contrast agents. In the case of Gd^{3+} MRI contrast agents the studies reported over the last two decades provide a plethora of data that enable rational control of some key physicochemical parameters. For instance, steric compression around the water coordination site was found to accelerate the water exchange process, by facilitating the dissociative water exchange reaction.[33] In the case of Mn^{2+} complexes the amount of data accumulated is far lower, so that the design of a potential MRI contrast agent on a rational basis is more difficult. We have shown here that increasing the steric compression around the water coordination site may have opposite effects on the water exchange rates of Gd^{3+} and Mn^{2+} complexes.

Experimental section

Materials and methods

NO2AtBu was purchased from CheMatech (Dijon, France). All other reagents and solvents were commercial samples and used without further purification. ^{1}H and ^{13}C NMR spectra were recorded at 25 °C on Bruker Avance 300 MHz and Bruker Avance 500 MHz spectrometers. High resolution electrospray-ionization time-of-flight (ESI-TOF) mass spectra were obtained in the positive mode using a LC-Q-q-TOF Applied Biosystems QSTAR Elite spectrometer. Elemental analyses were carried out on a ThermoQuest Flash EA 1112 elemental analyser. Medium performance liquid chromatography (MPLC) was carried out using a Puriflash XS 420 instrument equipped with a reverse-phase Puriflash 15C18HP column (60 Å, spherical 15 µm, 20 g) and UV-DAD detection at 210 and 254 nm, operating at a flow rate of 10 mL min^{-1}. Aqueous solutions were lyophilised using a Telstar Cryodos-80 apparatus.

Synthetic procedures

General procedure for the synthesis of the ligands. Triazacyclononane derivative NO2AtBu was dissolved in CH$_3$CN (20 mL) in the presence of K$_2$CO$_3$. A solution of the corresponding bromide precursor in CH$_3$CN (20 mL) was added dropwise to the suspension and the mixture was stirred for 48 h at room temperature. Once the alkylation was completed, the reaction mixture was filtered and the filtrate was concentrated under

vacuum at low temperature (30 °C) to afford yellowish oils that were characterised by ^{1}H and ^{13}C NMR and mass spectrometry (see details below), and used in the next step without further purification. The protected ligands were hydrolysed using a 1 : 1 TFA : CH$_2$Cl$_2$ mixture (8 mL), stirring at room temperature for 48 h. Once the deprotection was completed, the solution was concentrated *in vacuo* and washed several times with water (5 × 10 mL). The product was redissolved in water and lyophilised to obtain the final ligands.

Synthesis of di-*tert*-butyl 2,2′-(7-benzyl-1,4,7-triazonane-1,4-diyl)diacetate (H₂BzNO2A*t*Bu, 2a). This compound was obtained by using NO2A*t*Bu (0.2059 g, 0.5759 mmol), benzyl bromide (**1a**, 68.5 μL, 1 eq.) and K₂CO₃ (0.138 g, 1.73 eq.). Yellowish oil (0.260 g, quantitative). ^{1}H NMR (300 MHz, CDCl₃): δ_H (ppm): 7.31–7.25 (5H, m, CH$_{Ph}$), 3.67 (2H, m, CH₂), 3.30–3.24 (4H, m, CH₂), 2.93–2.80 (2H, m, CH₂), 1.45–1.38 (18H, m, CH₂); ^{13}C NMR (75 MHz, CDCl₃): δ_C (ppm) 171.46 (COO*t*Bu), 139.94 (C$_{Ph}$), 129.01 (C$_{Ph}$), 128.11 (C$_{Ph}$), 126.76 (C$_{Ph}$), 80.58 (–OC(CH₃)₃), 62.54 (CH₂), 59.85 (CH₂), 55.35 (CH₂), 55.15 (CH₂), 28.19 (CH₃). Mass spectrometry (ESI⁺) *m/z* (%BPI): 448.32 (100) ([C₂₄H₄₂N₃O₄]⁺).

Synthesis of 2,2′-(7-benzyl-1,4,7-triazonane-1,4-diyl)diacetic acid (H₂BzNO2Ac). Yellowish solid (0.3363 g, quantitative). ^{1}H NMR (300 MHz, D₂O): δ_H (ppm) 8.28 (3H, s, CH$_{Ph}$), 7.60 (1H, s, CH$_{Ph}$), 7.58 (2H, s, CH$_{Ph}$), 4.53 (4H, s, CH₂), 3.64–3.58 (8H, d, CH₂), 3.22 (6H, s, CH₂); ^{13}C NMR (75 MHz, D₂O): δ_C (ppm) 174.73 (COOH), 166.01 (C$_{Ph}$), 131.02 (C$_{Ph}$), 130.30 (C$_{Ph}$), 129.46 (C$_{Ph}$), 60.54 (CH₂), 57.55 (CH₂), 50.69 (CH₂), 50.45 (CH₂), 49.22 (CH₂). Mass spectrometry (ESI⁺) *m/z* (%BPI): 336.19 (100) ([C₁₇H₂₆N₃O₄]⁺), 358.17 (10) ([C₁₇H₂₅N₃NaO₄]⁺), 374.15 (7) ([C₁₇H₂₅KN₃NaO₄]⁺). HR-MS (ESI⁺) *m/z*: [M + Na]⁺, calculated: 336.1917, found: 336.1931.

Synthesis of di-*tert*-butyl 2,2′-(7-(1-phenylethyl)-1,4,7-triazonane-1,4-diyl)-diacetate (H₂MeBzNO2A*t*Bu, 2b). This compound was obtained using NO2A*t*Bu (0.2066 g, 0.578 mmol), α-methylbenzyl bromide (**1b**, 81.3 μL, 1 eq.) and K₂CO₃ (0.121 g, 1.5 eq.). Yellowish oil (0.267 g, quantitative). ^{1}H NMR (300 MHz, CDCl₃): δ_H (ppm) 7.34–7.32 (2H, d, CH$_{Ph}$), 7.27–7.22 (2H, t, CH$_{Ph}$), 7.18–7.13 (1H, t, CH$_{Ph}$), 3.79 (1H, s, CH), 3.24 (4H, s, CH₂), 2.90–2.69 (12H, m, CH₂), 1.40 (18H, s, CH₃), 1.32–1.31 (4H, d, CH₃). ^{13}C NMR (75 MHz, CDCl₃): δ_C (ppm) 171.48 (COO*t*Bu), 144.60 (C$_{Ph}$), 127.97 (C$_{Ph}$), 127.83 (C$_{Ph}$), 126.52 (C$_{Ph}$), 80.50 (–OC(CH₃)₃), 63.17 (CH), 59.58 (CH₂), 55.93 (CH₂), 55.20 (CH₂), 52.71 (CH₂), 28.18 (–OC(CH₃)₃). Mass spectrometry (ESI⁺) *m/z* (%BPI): 462.33 (100) ([C₂₆H₄₄N₃O₄]⁺), 406.27 (12) ([C₂₂H₃₆N₃O₄]⁺).

Synthesis of 2,2′-(7-(1-phenylethyl)-1,4,7-triazonane-1,4-diyl)diacetic acid (H₂MeBzNO2A). Yellowish solid (0.200 g, quantitative). ^{1}H NMR (300 MHz, D₂O): δ_H (ppm) 7.57–7.53 (5H, m, CH$_{Ph}$), 3.65 (16H, m, CH₂), 3.18 (1H, s, CH), 1.79–1.77 (3H, d, CH₂). ^{13}C NMR (75 MHz, D₂O): δ_C (ppm) 174.77 (COOH), 135.36 (C$_{Ph}$), 132.13 (C$_{Ph}$), 131.16 (C$_{Ph}$), 130.56 (C$_{Ph}$), 67.96 (CH), 57.75 (CH₂), 51.72 (CH₂), 50.86 (CH₂), 15.66 (CH₃). Mass spectrometry (ESI⁺) *m/z* (% BPI): 350.21 (100) ([C₁₈H₂₈N₃O₄]⁺), 372.19 (17) ([C₁₈H₂₇N₃NaO₄]⁺), 388.15 (12) ([C₁₈H₂₇KN₃O₄]⁺). HR-MS (ESI⁺) *m/z*: [M + Na]⁺, calculated: 350.2074, found: 350.2071.

Synthesis of tetra-*tert*-butyl 2,2′,2″,2‴-((1,3-phenylenebis(methylene))bis(1,4,7-triazonane-7,1,4-triyl))tetraacetate (*m*Bz(NO2A*t*Bu)₂, 2c). This compound was obtained using NO2A*t*Bu (0.3022 g, 0.8453 mmol), α,α′-dibromo-*m*-xylene (**1c**, 0.1151 g, 0.5 eq.) and K₂CO₃ (0.294, 5 eq.). Yellow oil (0.345 g, quantitative). ^{1}H NMR (300 MHz, CDCl₃): δ_H (ppm) 7.42 (1H, t, CH$_{Ph}$), 7.28–7.26 (2H, d, CH$_{Ph}$), 7.06–7.04 (1H, d, CH$_{Ph}$), 3.97 (2H, s, CH₂), 3.01–2.52 (30H, m, CH₂), 1.72–1.69 (4H, s, CH₂), 1.13–1.11 (36H, d, CH₃). ^{13}C NMR (75 MHz, CDCl₃): δ_C (ppm) 170.53 (COO*t*Bu), 131.54 (C$_{Ph}$), 129.95 (C$_{Ph}$), 129.00 (C$_{Ph}$), 116.45 (C$_{Ph}$), 81.00 (–OC(CH₃)₃), 59.86 (CH₂), 57.72 (CH₂), 52.48 (CH₂), 27.86 (–OC(CH₃)₃). Mass spectrometry (ESI⁺) *m/z* (%BPI): 817.58 (15) ([C₄₄H₇₇N₆O₈]⁺), 409.29 (100) ([C₄₄H₇₈N₆O₈]²⁺).

Synthesis of 2,2′,2″,2‴-((1,3-phenylenebis(methylene))bis(1,4,7-triazonane-7,1,4-triyl))tetraacetic acid (*m*Bz(H₂NO2A)₂). Reddish solid (0.250 g, quantitative). ^{1}H NMR (300 MHz, D₂O): δ_H (ppm) 7.66 (4H, m,

CH$_{Ph}$), 3.67–3.13 (32H, m, CH$_2$), 1.21 (4H, s, CH$_2$); ^{13}C NMR (75 MHz, D$_2$O): δ_C (ppm) 165.37–165.02 (COOH), 135.25 (C$_{Ph}$), 134.48 (C$_{Ph}$), 132.15 (C$_{Ph}$), 61.95 (CH$_2$), 52.33 (CH$_2$), 51.95 (CH$_2$), 50.81 (CH$_2$). Mass spectrometry (ESI$^+$) m/z (%BPI): 631.27 (100) ([C$_{28}$H$_{44}$KN$_6$O$_8$]$^+$), 593.33 (20) ([C$_{28}$H$_{45}$N$_6$O$_8$]$^+$), 669.22 (33) ([C$_{28}$H$_{43}$K$_2$N$_6$O$_8$]$^+$). HR-MS (ESI$^+$) m/z: [M + Na]$^+$, calculated: 593.3293, found: 593.3268.

General procedure for the synthesis of the complexes. The corresponding triazacyclononane ligand derivative was dissolved in *n*-BuOH (10 mL) in the presence of DIPEA (5 eq.) with the assistance of an ultrasonic bath. The solution was purged with an argon flow and afterwards the solid manganese salt, MnCl$_2$·4H$_2$O, was added. The reaction was maintained at 112 °C for 6 h. It was stopped and allowed to cool down to room temperature. The reaction mixture was concentrated under vacuum and redissolved in dichloromethane. The product was extracted with water (4 × 5 mL) and the aqueous phase was evaporated to furnish a yellowish solid. The solid was purified by MPLC using a reverse-phase C18 column. An aqueous solution of the compound under the eluting conditions (CH$_3$CN : H$_2$O, v : v, containing 0.1% triethylamine) was prepared and filtered through a cellulose filter (0.20 μm pore size) before injection. The purification method was carried out in a gradient of solvent B (CH$_3$CN, 5 to 10%) in solvent A (H$_2$O). The fractions containing the complex were combined and the solvent was removed under vacuum. The final product was redissolved in water and lyophilised to furnish the final complexes.

Synthesis of [Mn(BzNO2A)]. Yellowish solid (0.066 g, 34%). Mass spectrometry (ESI$^+$) m/z (%BPI): 411.1 (100) ([C$_{17}$H$_{23}$N$_3$O$_4$NaMn]$^+$). HR-MS (ESI$^+$) m/z: [M + Na]$^+$, calculated: 411.0961, found: 411.0954.

Synthesis of [Mn(MeBzNO2A)]. Yellowish solid (0.086 g, 37%). Mass spectrometry (ESI$^+$) m/z (%BPI): 425.11 (100) ([C$_{18}$H$_{25}$N$_3$O$_4$NaMn]$^+$), 403.13 (17) ([C$_{18}$H$_{26}$N$_3$O$_4$Mn]$^+$). HR-MS (ESI$^+$) m/z: [M + Na]$^+$, calculated: 425.1117, found: 425.1113.

Synthesis of [*m*Bz(MnNO2A)$_2$]. Yellowish solid (0.090 g, 39%). Mass spectrometry (ESI$^+$) m/z (%BPI): 721.16 (100) ([C$_{28}$H$_{40}$N$_6$O$_8$NaMn$_2$]$^+$), 699.18 (8) ([C$_{28}$H$_{41}$N$_6$O$_8$Mn$_2$]$^+$). HR-MS (ESI$^+$) m/z: [M + Na]$^+$, calculated: 721.1560, found: 721.1551.

^{1}H NMRD and ^{17}O NMR measurements

The proton $1/T_1$ NMRD profiles were measured on a fast field-cycling Stelar SmartTracer relaxometer (Mede, Pv, Italy) over a continuum of magnetic field strengths from 0.00024 to 0.25 T (corresponding to 0.01–10 MHz proton Larmor frequencies). The relaxometer operates under computer control with an absolute uncertainty in $1/T_1$ of ±1%. The temperature control was carried out using a Stelar VTC-91 airflow heater equipped with a calibrated copper-constantan thermocouple (uncertainty of ±0.1 K). Additional data points in the range 20–60 MHz were obtained on a Stelar Relaxometer equipped with a Bruker WP80 NMR electromagnet adapted to variable-field measurements (15–80 MHz proton Larmor frequency). The exact complex concentration was determined by the BMS shift method at 11.7 T.[34] ^{17}O NMR measurements were recorded on a Bruker Avance III spectrometer (11.7 T) equipped with a 5 mm probe and a standard temperature control unit. Aqueous solutions of the complexes (*ca.* 6–10 mM) containing 2.0% of the ^{17}O isotope (Cambridge Isotope) were used. The observed transverse relaxation rates were calculated from the signal width at a half-height.

pH stability range

Solutions of [Mn(BzNO2A)], [Mn(MeBzNO2A)] and [*m*Bz(MnNO2A)$_2$] (1 mM) were prepared in the pH range 1.72–10.5. The longitudinal relaxation rates were measured at 20 MHz and 298 K. The measurements were carried out in a BrukerMinispec MQ 20.

<u>Computational details</u>

Full geometry optimisation of the [Mn(MeNO2A)(H$_2$O)]·xH$_2$O (x = 2, 5), [Mn(BzNO2A)(H$_2$O)]·2H$_2$O, [Mn(MeBzNO2A)(H$_2$O)]·2H$_2$O and [mBz(MnNO2A)$_2$]·3H$_2$O systems was performed employing DFT calculations at the M06-2X/TZVP[35,36] level employing the Gaussian 09 package (Revision E.01).[37] Solvent effects (water) were introduced by using the integral equation formalism variant of the polarizable continuum model (IEFPCM).[38] No symmetry constraints were imposed during the optimisation processes. All stationary points found as a result of geometry optimisation were confirmed to represent the energy minima on the potential energy surfaces *via* frequency analysis. [17]O hyperfine coupling constants were calculated using the M06-2X functional in combination with the aug-cc-pVTZ-J basis set for Mn[39] and the EPR-III[40] basis set for the ligand atoms.

The potential energy surface of the [Mn(MeNO2A)(H$_2$O)]·5H$_2$O system was investigated by performing relaxed potential energy surface scans, which were generated by either: (i) increasing the distance between Mn and the oxygen atom of the coordinated water molecule in steps of 0.1 Å, or (ii) shortening the distance between a second-sphere water molecule and the Mn atom in steps of 0.1 Å. The geometries generated from these calculations were subsequently used to calculate the transition state characterising the associative water exchange mechanisms with the aid of the synchronous transit-guided quasi-Newton approach.[41] Saddle points were characterised using frequency calculations, which also provided zero-point energies (ZPEs), enthalpies (*H*) and free energies (*G*) at 298.15 K and 1 atm.

Conflicts of interest

There are no conflicts of interest to declare.

Acknowledgements

References

01   (*a*) J. Wahsner, E. M. Gale, A. Rodríguez-Rodríguez and P. Caravan, *Chem. Rev.*, 2019, **119**, 957. (*b*) A. Merbach, L. Helm and E. Tóth, *The Chemistry of Contrast Agents in Medical Magnetic Resonance Imaging*, John Wiley & Sons, Chichester, 2013.

02   (*a*) L. Helm, J. R. Morrow, C. J. Bond, F. Carniato, M. Botta, M. Braun, Z. Baranyai, R. Pujales-Paradela, M. Regueiro-Figueroa, D. Esteban-Gómez, C. Platas-Iglesias and T. J. Scholl, *Contrast Agents for MRI. Experimental Methods*, V. C. Pierre and M. J. Allen, Royal Society of Chemistry, Croydon, UK, 2018. (*b*) B. Phukan, C. Mukherjee, U. Goswami, A. Sarmah, S. Mukherjee, S. K. Sahoo and S. Ch. Moi, *Inorg. Chem.*, 2018, **57**, 2631.

03   (*a*) S. Cheng, L. Abramova, G. Saab, G. Turabelidze, P. Patel, M. Arduino, T. Hess, A. Kallen and M. Jhung, *J. Am. Med. Assoc.*, 2007, **297**, 1542. (*b*) T. H. Darrah, J. J. Prutsman-Pfeiffer, R. J. Poreda, M. E. Campbell, P. V. Hauschka and R. E. Hannigan, *Metallomics*, 2009, **1**, 479.

04   (*a*) D. R. Roberts, S. M. Lindhorst, C. T. Welsh, K. R. Maravilla, M. N. Herring, K. A. Braun, B. H. Thiers and W. C. Davis, *Invest. Radiol.*, 2016, **51**, 280. (*b*) M. Birka, K. S. Wentker, E. Lusmöller, B. Arheilger, C. A. Wehe, M. Sperling, R. Stadler and U. Karst, *Anal. Chem.*, 2015, **87**, 3321. (*c*) T. Kanda, T. Fukusato, M. Matsuda, K. Toyoda, H. Oba, J. Kotoku, T. Haruyama, K. Kitajima and S. Furui, *Radiology*, 2015, **276**, 228. (*d*) E. Kanal and M. F. Tweedle, *Radiology*, 2015, **275**, 630. (*e*) T. J. Fraum, D. R. Ludwig, M. R. Bashir and K. J. Fowler, *J. Magn. Reson. Imaging*, 2017, **46**, 338.

05   V. M. Runge *Invest. Radiol.*, 2018, **53**, 571.

06   (*a*) D. Pan, A. H. Schmieder, S. A. Wickline and G. M. Lanza, *Tetrahedron*, 2011, **67**, 8431. (*b*) B. Drahos, I. Lukes and E. Toth, *Eur. J. Inorg. Chem.*, 2012, 1975. (*c*) M. Kueny-Stotz, A. Garofalo and D. Felder-Flesch, *Eur. J. Inorg. Chem.*, 2012, 1987.

07   J. R. Morrow and E. Toth, *Inorg. Chem.*, 2017, **56**, 6029.

08   E. M. Gale, I. P. Atanasova, F. Blasi, I. Ay and P. Caravan, *J. Am. Chem. Soc.*, 2015, **137**, 15548.

09   (*a*) J. Zhu, E. M. Gale, I. Atanasova, T. A. Rietz and P. Caravan, *Chem. – Eur. J.*, 2014, **20**, 14507. (*b*) B. Phukan, A. B. Patel and C. Mukherjee, *Dalton Trans.*, 2015, **44**, 12990. (*c*) H. Su, C. Wu, J. Zhu, T. Miao, D. Wang, C. Xia, X. Zhao, Q. Gong, B. Song and H. Ai, *Dalton Trans.*, 2012, **41**, 14480.

10   (*a*) M. Regueiro-Figueroa, G. A. Rolla, D. Esteban-Gomez, A. de Blas, T. Rodriguez-Blas, M. Botta and C. Platas-Iglesias, *Chem. – Eur. J.*, 2014, **20**, 17300. (*b*) A. Forgacs, M. Regueiro-Figueroa, J. L. Barriada, D. Esteban-Gomez, A. de Blas, T. Rodriguez-Blas, M. Botta and C. Platas-Iglesias, *Inorg. Chem.*, 2015, **54**, 9576. (*c*) A. Forgács, L. Tei, Z. Baranyai, D. Esteban-Gómez, C. Platas-Iglesias and M. Botta, *Dalton Trans.*, 2017, **46**, 8494. (*d*) R. Pujales-Paradela, F. Carniato, R. Uzal-Varela, I. Brandariz, E. Iglesias, C. Platas-Iglesias, M. Botta and D. Esteban-Gomez, *Dalton Trans.*, 2019, **48**, 696.

11   G. F. Kwakye, M. M. B. Paoliello, S. Mukhopadhyay, A. B. Bowman and M. Aschner, *Int. J. Environ. Res. Public Health*, 2015, **12**, 7519.

12   (*a*) G. L. Loving, S. Mukherjee and P. Caravan, *J. Am. Chem. Soc.*, 2013, **135**, 4620. (*b*) E. M. Gale, S. Mukherjee, C. Liu, G. S. Loving and P. Caravan, *Inorg. Chem.*, 2014, **53**, 10748.

13   (*a*) Z. Baranyai, Z. Palinkas, F. Uggeri, A. Maiocchi, S. Aime and E. Brucher, *Chem. – Eur. J.*, 2012, **18**, 16426. (*b*) Z. Baranyai, E. Brucher, F. Uggeri, A. Maiocchi, I. Toth, M. Andrasi, A. Gaspar, L. Zekany and S. Aime, *Chem. – Eur. J.*, 2015, **21**, 4789.

14   E. Balogh, Z. He, W. Hsieh, S. Liu and É. Tóth, *Inorg. Chem.*, 2007, **46**, 238.

15   (*a*) Y. Ducommun, K. E. Newman and A. E. Merbach, *Inorg. Chem.*, 1980, **19**, 3696. (*b*) D. Esteban-Gómez, C. Cassino, M. Botta and C. Platas-Iglesias, *RSC Adv.*, 2014, **4**, 7094.

16   V. Patinec, G. A. Rolla, M. Botta, R. Tripier, D. Esteban-Gomez and C. Platas-Iglesias, *Inorg. Chem.*, 2013, **52**, 11173.

17   A. de Sá, C. S. Bonnet, C. F. G. C. Geraldes, É. Tóth, P. M. T. Ferreira and J. P. André, *Dalton Trans.*, 2013, **42**, 4522.

18   S. Aime, M. Botta, D. Esteban-Gómez and C. Platas-Iglesias, *Mol. Phys.*, 2018.

19   G. A. Rolla, C. Platas-Iglesias, M. Botta, L. Tei and L. Helm, *Inorg. Chem.*, 2013, **52**, 3268.

20   L. Tei, G. Gugliotta, M. Fekete, F. K. Kalman and M. Botta, *Dalton Trans.*, 2011, **40**, 2025.

21   (*a*) S. Aime, A. Barge, J. I. Bruice, M. Botta, J. A. K. Howard, J. M. Moloney, D. Parker, A. S. de Sousa and M. Woods, *J. Am. Chem. Soc.*, 1999, **121**, 576. (*b*) S. Aime, A. Barge, M. Botta, D. Parker and A. S. De Sousa, *J. Am. Chem. Soc.*, 1997, **119**, 4767. (*c*) A. Rodriguez-Rodriguez, M. Regueiro-Figueroa, D. Esteban-Gomez, T. Rodriguez-Blas, V. Patinec, R. Tripier, G. Tircso, F. Carniato, M. Botta and C. Platas-Iglesias, *Chem. – Eur. J.*, 2017, **23**, 1110.

22   S. Aime, A. Barge, J. I. Bruce, M. Botta, J. A. K. Howard, J. M. Moloney, D. Parker, A. S. de Sousa and M. Woods, *J. Am. Chem. Soc.*, 1999, **121**, 5762.

23   J. A. Peters and C. F. G. C. Geraldes, *Inorganics*, 2018, **6**, 116.

24   E. M. Gale, J. Zhu and P. Caravan, *J. Am. Chem. Soc.*, 2013, **135**, 18600.

25   C. Platas-Iglesias, D. Esteban-Gómez, L. Helm and M. Regueiro-Figueroa, *J. Phys. Chem. A*, 2016, **120**, 6467.

26   (*a*) I. Solomon and N. Bloembergen, *J. Chem. Phys.*, 1956, **25**, 261. (*b*) N. Bloembergen and L. O. Morgan, *J. Chem. Phys.*, 1961, **34**, 842.

27   J. H. Freed *J. Chem. Phys.*, 1978, **68**, 4034.

28   R. Pujales-Paradela, M. Regueiro-Figueroa, D. Esteban-Gómez and C. Platas-Iglesias, *Contrast Agents for MRI. Experimental Methods*, V. C. Pierre and M. J. Allen, Royal Society of Chemistry, Croydon, UK, 2018.

29   (*a*) E. Molnar, N. Camus, V. Patinec, G. A. Rolla, M. Botta, G. Tircso, F. K. Kalman, T. Fodor, R. Tripier and C. Platas-Iglesias, *Inorg. Chem.*, 2014, **53**, 5136. (*b*) M. Khannam, T. Weyhermüller, U. Goswami and C. Mukherjee, *Dalton Trans.*, 2017, **46**, 10426.

30   L. Leone, D. Esteban-Gomez, C. Platas-Iglesias, M. Milanesio and L. Tei, *Chem. Commun.*, 2019, **55**, 513.

31   K. Pota, Z. Garda, F. K. Kalman, J. L. Barriada, D. Esteban-Gomez, C. Platas-Iglesias, I. Toth, E. Brucher and G. Tircso, *New J. Chem.*, 2018, **42**, 8001.

32   (*a*) C. D. Hubbard and R. van Eldik, *Inorg. Chim. Acta*, 2010, **363**, 2357. (*b*) L. Helm and A. E. Merbach, *Chem. Rev.*, 2005, **105**, 1923.

33   (*a*) S. Laus, R. Ruloff, E. Toth and A. E. Merbach, *Chem. – Eur. J.*, 2003, **9**, 3555. (*b*) L. Tei, G. Gugliotta, Z. Baranyai and M. Botta, *Dalton Trans.*, 2009, 9712. (*c*) E. Balogh, M. Mato-Iglesias, C. Platas-Iglesias, E. Toth, K. Djanashvili, J. A. Peters, A. de Blas and T. Rodríguez-Blas, *Inorg. Chem.*, 2006, **45**, 8719. (*d*) J. Kotek, P. Lebduskova, P. Hermann, L. Vander Elst, R. N. Muller, C. F. G. C. Geraldes, T. Maschmeyer, I. Lukes and J. A. Peters, *Chem. – Eur. J.*, 2003, **9**, 5899.

34   D. M. Corsi, C. Platas-Iglesias, H. van Bekkum and J. A. Peters, *Magn. Reson. Chem.*, 2001, **39**, 723.

35   Y. Zhao and D. G. Truhlar, *Theor. Chem. Acc.*, 2008, **120**, 215.

36   A. Schaefer, C. Huber and R. Ahlrichs, *J. Chem. Phys.*, 1994, **100**, 5829.

37   M. J.Frisch, G. W.Trucks, H. B.Schlegel, G. E.Scuseria, M. A.Robb, J. R.Cheeseman, G.Scalmani, V.Barone, G. A.Petersson, H.Nakatsuji, X.Li, M.Caricato, A.Marenich, J.Bloino, B. G.Janesko, R.Gomperts, B.Mennucci, H. P.Hratchian, J. V.Ortiz, A. F.Izmaylov, J. L.Sonnenberg, D.Williams-Young, F.Ding, F.Lipparini, F.Egidi, J.Goings, B.Peng, A.Petrone, T.Henderson, D.Ranasinghe, V. G.Zakrzewski, J.Gao, N.Rega, G.Zheng, W.Liang, M.Hada, M.Ehara, K.Toyota, R.Fukuda, J.Hasegawa, M.Ishida, T.Nakajima, Y.Honda, O.Kitao, H.Nakai, T.Vreven, K.Throssell, J. A.Montgomery Jr., J. E.Peralta, F.Ogliaro, M.Bearpark, J. J.Heyd, E.Brothers, K. N.Kudin, V. N.Staroverov, T.Keith, R.Kobayashi, J.Normand, K.Raghavachari, A.Rendell, J. C.Burant, S. S.Iyengar, J.Tomasi, M.Cossi, J. M.Millam, M.Klene, C.Adamo, R.Cammi, J. W.Ochterski, R. L.Martin, K.Morokuma, O.Farkas, J. B.Foresman and D. J.Fox, Gaussian 09, Revision E.01, Gaussian, Inc., Wallingford CT, 2016.

38   J. Tomasi, B. Mennucci and R. Cammi, *Chem. Rev.*, 2005, **105**, 2999.

39   E. D. Hedegard, J. Kongsted and S. P. A. Sauer, *J. Chem. Theory Comput.*, 2011, **7**, 4077.

40   N. Rega, M. Cossi and V. Barone, *J. Chem. Phys.*, 1996, **105**, 11060.

41   (*a*) C. Peng and H. B. Schlegel, *Isr. J. Chem.*, 1993, **33**, 449. (*b*) C. Peng, P. Y. Ayala, H. B. Schlegel and M. J. Frisch, *J. Comput. Chem.*, 1995, **16**, 49.

[i] Electronic supplementary information (ESI) available: ^{1}H NMR, ^{13}C NMR and mass spectra of the ligands and their precursors and complexes, equations used for the analysis of ^{1}H and ^{17}O NMR data and optimised Cartesian coordinates obtained with DFT calculations. See DOI: 10.1039/c9dt00211a.